



1

2 **Towards a monitoring system of temperature extremes in Europe**

3 Christophe Lavaysse¹, Carmelo Cammalleri¹, Alessandro Dosio¹, Gerard van der Schrier², Andrea Toreti¹ and
4 Jürgen Vogt¹

5

6 Affiliations:

7 1- European Commission, Joint Research Centre (JRC), Ispra, Italy

8 2- Royal Netherlands Meteorological Institute (KNMI), De Bilt, The Netherlands

9

10

11 Abstract

12 Extreme temperature anomalies such as heat and cold waves may have strong impacts on human activities and
13 health. The heat waves in Western Europe in 2003 and in Russia in 2010, or the cold wave in South-Eastern
14 Europe in 2012, generated a considerable amount of economic loss and resulted in the death of several
15 thousands of people. Providing an operational system to monitor extreme temperature anomalies in Europe is
16 thus of prime importance to help decision makers and emergency services which are responsive to an
17 unfolding extreme event.

18 In this study, the development and the validation of a monitoring system of extreme temperature anomalies
19 are presented. The first part of the study describes the methodology based on the persistence of events
20 exceeding a percentile threshold. The method is applied to three different observational datasets, in order to
21 assess the robustness and highlighting uncertainties in the observations. The climatology of extreme events
22 from the last 21 years is then analysed to highlight the spatial and temporal variability of the hazard and
23 discrepancies amongst the observational datasets are discussed. In the last part of the study, the products
24 derived from this study are presented and discussed regarding previous studies. The results highlight the
25 accuracy of the developed index and the statistical robustness of the distribution used to calculate the return
26 periods.

27

28

29

30

31 Key words: Monitoring heat waves, EOBS, ERAI, Europe

32 Corresponding author: Christophe Lavaysse, European Commission, Joint Research Centre (JRC), Directorate
33 for Space, Security and Migration, Disaster Risk Management Unit, Via E. Fermi 2749, I-21027 Ispra (VA),
34 Italy

35 Christophe.lavaysse@ec.europa.eu



36 1 Introduction

37 Extreme temperature anomalies have strong impacts on human health and activities. The heat waves that
38 occurred over Western Europe in August 2003 caused about 70,000 deaths across twelve countries (Robine et
39 al. 2008). The heat wave in Russia during the summer 2010, considered as the strongest in the last 30 years
40 (Barriopedro et al. 2011, Russo et al 2015), caused more than 55,000 victims and 500 billion euro of damage.
41 In February 2012 a cold wave over Central and Eastern Europe generated more than 700 million euro of
42 damage, and 825 deaths were reported (de'Donato et al., 2013). Monitoring and cataloguing these events are
43 crucial in order to place an event in the historic perspective and in order to assess the potential impacts on
44 human health and activities by combining the information with data from other catalogues (such as EM-DAT,
45 <http://www.emdat.be>). A catalogue would also be appropriate to analyse the spatial and temporal evolutions
46 of the hazard related to temperature anomalies, and, finally in the future, to calibrate and validate an
47 operational forecasting system in terms of these extreme events. This product will be implemented in the
48 operational monitoring system of the European Drought Observatory (EDO, <http://edo.jrc.ec.europa.eu>).

49 From the human health point of view, a heat (cold) wave can be considered as a period with sustained
50 temperature anomalies resulting in one of a number of health outcomes, including mortality, morbidity and
51 emergency service call-out (Kovats et al., 2006). Wave intensity and duration, but also time of the year, are
52 important determinants of the impact on health (Montero et al., 2012; Rocklov et al., 2012). While most studies
53 focus on daytime conditions only, there is emerging evidences that nocturnal conditions can also play an
54 important role in generating heat-related health effects, a result of the cumulative build-up of the heat load
55 with little respite during the night (Rooney et al., 1998).

56 In the literature, some indicators have been developed to describe the complex conditions of heat exchange
57 between the human body and its thermal environment. For warm conditions, indices usually consist of
58 combinations of dry-bulb temperature and different measures for humidity or wind speed, such as: the
59 humidex (Smoyer-Tomic et al. 2003), the net effective temperature (Li and Chan, 2000), the wet-bulb globe
60 temperature (Budd, 2009), the heat index (Steadman, 1979) or the apparent temperature (Steadman, 1984).
61 More generally, efforts have been made to harmonize the large number of indices developed. For example,
62 the Universal Thermal Climate Index (UCTI, www.utci.org) has been proposed to assess heat and cold waves.
63 The main inconvenience of most of these indices is technical, i.e., the humidity when the daily maximum or
64 daily minimum temperature (hereafter Tmax and Tmin) occur is not necessarily known. In addition, the
65 simulate values of wind speed and humidity provided by numerical weather models are generally less accurate
66 than the 2m temperature in the reanalysis and observational datasets. The WMO Expert Team on Climate
67 Change Detection and Indices (ETCCDI) proposed the Warm Spell Duration Index (WSDI) as standard
68 measurement of heat and cold waves which is calculated using a percentile-based threshold. Russo et al. (2015)
69 proposed a version of this method that provides the amplitude (or intensity) of a heat wave based on the
70 maximum temperature and the interquartile range of yearly maximum temperature of the past period. This
71 method is powerful to compare the heatwaves at climatological scale over the world and their trends with a
72 local standardization. Nevertheless, this method is not suitable for monitoring heat waves because it focuses



73 on the most extreme events (the thresholds are defined according to the yearly maximums), and it does not
74 take into account the Tmin that has a strong human impact according to WMO (2015).

75 In this study we propose an operational system to monitor heat and cold waves based on an adapted index
76 inspired by the previous studies. In section 2, data and methods are presented and the uncertainties related to
77 the observations are assessed. Then, the climatology in term of occurrence, intensity and duration of the waves
78 are presented in section 3. This represents the baseline of the monitoring system that will become operational
79 and embedded in the EDO system. Finally, concluding remarks are provided in section 4.

80

81 **2 Data and tools**

82 **2.1 Datasets**

83 In this study we use daily Tmax and Tmin from three different datasets. The first one is based on the 2m
84 temperature datasets provided by the European National Weather Services, which, in turn, is used as an input
85 for the LisFlood hydrological model (De Roo et al., 2000). The observations are gridded onto a regular lat/lon
86 grid of one square degree. The use of gridded observation data is motivated i) to focus on large scales heat/cold
87 waves and ii) to compare the station data with reanalysis. This LisFlood product will be eventually used in the
88 operational system for the monitoring of extreme temperature waves. To validate the results, a comparison
89 with two other sets of data is performed: the ERA-Interim reanalysis (ERA-Interim, Dee et al., 2011) and the
90 EObs/ECAD dataset Version 14 (Haylock et al., 2008, van den Besselaar et al., 2011), both regridded to the
91 same one square degree resolution. Note that, according to ECMWF, ERA-Interim datasets are released with a delay
92 of two months for quality assurance; as a consequence this dataset cannot be used for operational monitoring
93 purpose. The same problem occurs for the EObs datasets.

94 The definition of Tmax and Tmin in the three datasets can differ from the definition of WMO (van den
95 Besselaar et al. 2012). In LisFlood, the Tmin assigned to the day d is defined as the minimum temperature
96 value that occurred from 1800Local Time (LT) of the day before (d-1) to 0600LT of the day d. For EObs,
97 Tmin is defined as the 24-hour daily minimum. Similarly, Tmax of the day d is the maximum temperature
98 recorded from 0600LT to 1800LT of the day d for LisFlood data and the 24-hour daily maximum for EObs.
99 In ERA-Interim, Tmin (Tmax) of day d is the lowest (highest) value of temperatures recorded at 0000LT, 0600LT,
100 1200LT or 1800LT of day d. The starting years of the period covered by the datasets are also different (1950
101 for EObs, 1979 for ERA-Interim and 1990 for LisFlood). In order to be consistent and in a view of the future use for
102 the reforecast period of the ECMWF ENS forecast model, the period from 1995 to 2015 (21 years) is used for
103 all the datasets. Note that most of the results obtained in this study have been compared to a longer period
104 (starting from 1990) providing very similar results.

105 **2.2 Metric of extreme temperature anomalies**

106 Following the WMO definition, there are many different ways to measure a heat wave (Perkins et al., 2013).
107 The objective of this study is not to create a new index, but to provide an operational system based on an



108 adapted method proposed in the literature. This system is inspired by the studies of Russo et al., (2014) and
109 WMO (2015). First, daily T_{min} and T_{max} are transformed into quantiles based on the climatological (21
110 years) calendar percentiles of each variable. To highlight the events with the most potential human impacts,
111 the year is cut in two periods: The extended summer period, when heat waves could have more impacts (6
112 hottest month over Europe, from April to September), and the extended winter period to focus on the cold
113 waves (from October to March). Note that also during the summer (winter) period, cold (heat) waves may
114 occur but they are not considered here. The independent calculation of the daily quantiles of observed T_{min}
115 and T_{max} is done by applying a leave-one-out method to avoid inhomogeneities (Zhang et al. 2005). The year
116 studied is removed from the climatology. The data without this year is exploited to perform the observed
117 cumulative distribution function (CDF). To remove artefacts due to the relative small sampling (21 years), a
118 window of 11 days centred on the day studied is exploited. The daily temperatures are transformed into
119 quantile by this procedure to create two daily temperature quantiles from 1995 to 2015, derived from the CDF
120 of T_{min} and T_{max} independently.

121 The main difference with the previous studies is the use of both T_{max} and T_{min}, rather than T_{max} only or the
122 daily mean temperature. Then a hot day is defined when simultaneously the daily quantiles of T_{max} and T_{min}
123 are above quantile 0.9 during the extended summer (from April to September). The same definition is applied
124 for cold days when the two quantiles are lower than quantile 0.1 from October to March. The occurrences are
125 strongly influenced by these thresholds. As this study aims at quantifying the intensity of waves regarding the
126 climatology and at assessing with robust scores the forecast of these events, it is not possible to focus only on
127 the most extreme cases. So these thresholds (quantiles 0.9 and 0.1) are chosen as compromise between the
128 need to have a minimum number of events and the definition of extremes. They are also used in a large number
129 of other studies (WMO, 2015, Hirschi et al., 2011). Note that in order to discuss the sensitivity of using the
130 intersection of T_{min} and T_{max} rather than one temperature value per day, the same methodology has also
131 been applied using only T_{min} and only T_{max} to determined hot and cold days.

132 Heat and cold waves are associated with a persistence of hot or cold days. Based on the literature (Gasparri
133 and Armstrong, 2011, Kuglitsch et al, 2010), as well as on the recommendation of WMO (2015) for health
134 impacts, we define a heat (cold) wave as an event of at least 3 consecutive hot (cold) days (i.e. when
135 simultaneously T_{min} and T_{max} exceed the quantile thresholds). A pool is also introduced when two events
136 are separated by less than one day. Note that periods in between two waves are not taken into account in the
137 wave duration and in the wave intensity. Fig. 1 illustrates the method used to detect heat waves in this study.

138 The European mean distribution of these cases are presented in Table 1 and 2 using the LisFlood dataset, but
139 the results are very similar with the two others datasets (not shown). The table demonstrate the impact of using
140 the intersection of T_{min} and T_{max} above (below) the thresholds. With respect to heat waves (Table 1), for
141 example, about 150 out of 376 days, i.e. 40% of the T_{min} above the thresholds occurred simultaneously (i.e.
142 the same day) with T_{max} above the threshold (Table 1, first column). Even if the differences are not large,
143 there is another result with a significant more persistency of T_{max} than T_{min}. For instance, using T_{max} only,
144 70% of the hot days (269 out of the 382) are detected as being part of a heat wave, whereas using T_{min} only,



145 the ratio is about 60% (i.e. 226 out of 376). Using both Tmax and Tmin, on average 81.3 days (54% of the hot
 146 days) are detected as being part of a heat wave (Table 1, second column). Finally, the mean occurrences of
 147 heat waves are indicated in the last column. The use of the two temperatures tends to reduce drastically the
 148 number of events (from 44 or 51 to 16.9 on average during the period) but also their durations (5.11 or 5.3
 149 days to 4.8). The continental regions appear less affected by this reduction than coastal regions (not shown).
 150 In analogy, Table 2 shows the same data for the case of cold waves.

151 Once a wave is detected, two main characteristics are recorded: the duration (in days) and the intensity. To
 152 take into account different characteristics and to assess the sensitivity of the methods, the latter is calculated
 153 by three different methods. The first one is based on the sum of the quantiles above (or under) the threshold
 154 during the detected wave.

155

$$156 \quad I1(n) = \sum_{i=1}^N \beta \frac{[Qtx_{i,w} - Thres + Qtn_{i,w} - Thres]}{2} \begin{cases} \beta = 1 \text{ for Heat waves} \\ \beta = -1 \text{ for cold waves} \end{cases}$$

157

158 Where $I1$ is the intensity of the wave having duration equal to N days, Qtn and Qtx the daily quantile of Tmin
 159 and Tmax and $Thres$, the quantile thresholds (i.e. 0.9 and 0.1 for heat and cold days respectively). The purpose
 160 of dividing this intensity by 2 is to create an intensity comparable to the intensities calculated with Tmin and
 161 Tmax only. The second method is similar to the first but the quantile differences are replaced by the
 162 temperature anomalies with respect to the climatological daily thresholds. This method is defined as follows:

163

$$164 \quad I2(n) = \sum_{i=1}^N \beta \frac{[Tx_{i,w} - Q_{Tx} + Tn_{i,w} - Q_{Tn}]}{2} \begin{cases} \beta = 1 \text{ for Heat waves} \\ \beta = -1 \text{ for cold waves} \end{cases}$$

165 Where Q_{Tx} and Q_{Tn} represent the calendar daily thresholds of Tmax and Tmin, i.e. the temperatures for the
 166 quantiles 0.9 (0.1) for the heat (cold respectively) waves. This method allows quantifying intensities regarding
 167 the seasonal cycle and reflects an anomaly but not necessarily extreme values of absolute temperatures. This
 168 calculation is motivated for agricultural applications, where the yield crops can be sensitive to these large
 169 anomalies during the transitional seasons (Porter and Semenov, 2005). The last method is also based on
 170 temperature anomalies but regarding a constant threshold.

171

$$172 \quad I3(n) = \sum_{i=1}^N \beta * \left[\frac{[Tx_{i,w} - Tx_{med(Q_{Tx})}]}{2 * \sigma_{Tx}} + \frac{[Tn_{i,w} - Tn_{med(Q_{Tn})}]}{2 * \sigma_{Tn}} \right] \begin{cases} \beta = 1 \text{ for Heat waves} \\ \beta = -1 \text{ for cold waves} \end{cases}$$

173



174 Where $Tx_{med(QTx)}$ and $Tn_{med(QTn)}$ represent the constant temperature of the median of all the calendar daily
175 quantiles of 0.9 (heat waves) and 0.1 (cold waves) of Tmax and Tmin. σ_{Tx} and σ_{Tn} represent the
176 climatological yearly variance of Tmax and Tmin. This method is intended to increase the intensities of a
177 heat or cold waves that occur close to the maximum or minimum of the seasonal cycle. Based on this
178 calculation, the strongest intensities are generally associated with the warmest or coldest absolute
179 temperatures. The division by the variance of the seasonal cycle is justified to reduce the intensity of the waves
180 that occurred over region with strong seasonal cycle, where the variability of temperature is well known to be
181 variable. The latter method is conceptually close to the one proposed by Russo et al. (2015) and, due to its
182 sensitivity to the absolute temperatures, could be more suitable to assess the potential impacts on human
183 health. Fig.1 illustrates the heat wave detection and the calculation of the two last methodologies. The different
184 intensities provided by these three methods, which use the same detection method, are discussed in the results
185 section.

186

187 **3 Results**

188 **3.1 Comparison of the datasets**

189 In order to compare the observations and quantify the uncertainties of the results, different datasets, provided
190 by observations and reanalysis, are used. First, the temporal correlations between different pairs of the daily
191 quantiles are shown in Fig. 2. We notice that the correlation of the quantiles of Tmin and Tmax from ERAI,
192 EOBS and LisFlood datasets are quite in agreement (the spatial mean correlation is about 0.89). Note that as
193 the quantiles are used, the seasonal cycle is removed, showing the quality of this agreement. The scores are
194 generally better for Tmax than Tmin. This could be explained by the larger spatial homogeneity of Tmax than
195 Tmin and the differences in the Tmin definition amongst National Weather Services. Indeed, over certain
196 countries, Tmin is measured during night time between 1800LT and 0600LT the following day, elsewhere
197 from 0000LT to 2400LT or from 0600LT day d to 0600LT day d+1, which could result in a delay of one day.
198 In the EOBS data description, and in van den Besselaar et al. (2011), this point and the uncertainties associated
199 are deeply analysed. Due to the coarser resolution and only 4 recorded values per day to calculate Tmin and
200 Tmax, ERAI is associated with a hot bias of Tmin and a cold bias of Tmax in relation to both LisFlood and
201 EOBS datasets (not shown). The yearly Mean Absolute Errors of Tmin and Tmax (MAE, Fig. 3, very close
202 to the Root Mean Square Differences) remains, however, relatively low (<1.5 deg.) except at the borders of
203 the domain, confirming the good agreement especially between EOBS and ERAI. Note that the LisFlood
204 dataset is slightly less correlated to the others over Scandinavia, Germany and on the North-easternmost part
205 of the domain probably due to the definition of Tmin and Tmax for each country, delay in the GTS
206 communications and the density of the stations (the E-OBS network over Germany and Scandinavia is quite
207 dense).



208 3.2 Climatology

209 3.2.1 Occurrence variabilities of the waves

210 The total occurrences of heat and cold waves during the 21 years are calculated using the definition presented
211 in section 2. This is performed independently for the three datasets to provide information on the robustness
212 of the results. As shown in Table 1 and 2 cold waves are more frequent than heat waves for the three datasets
213 especially in the eastern part of Europe (Fig. 4 and 5, first row). The same figures using independently only
214 Tmin or Tmax to detect both heat and cold waves reveal more homogeneous spatial patterns and quite the
215 same number of occurrence between them, but about 50 to 60% more than the intersection of Tmin and Tmax
216 (Fig. 4 and 5 second and third row). Only the detection of the heat waves using Tmin only generate less events.
217 These results highlight two main characteristics: 1) the lower persistency of Tmin with strong positive
218 anomalies could partially explain the difference between the occurrence of heat and cold waves; 2) the increase
219 of the occurrence in the continental regions is mainly explained by an increase of the simultaneous anomalies
220 in Tmin and Tmax rather than an increase of occurrence of persistency. These two characteristics may be
221 explained by the synoptical situations during cold waves and the fact that there are more frequent
222 meteorological blocking conditions in winter than in summer (Tibaldi et al. 1994, Doblas-Reyes et al, 2002).
223 Several recent studies (Tomczyk and Bednorz 2016, Sousa et al. 2017) emphasized the important role of
224 persistent and intense blocking and associated anticyclones in producing heat or cold waves. The origins of
225 the extreme blocking situations are still not well understood and could be related to the development of a
226 large-scale Rossby train (Trenberth and Fasullo 2012). Finally the study of Schubert et al. (2014), who
227 identified Western Russia as the leading mode of surface temperature and precipitation covariability could
228 highlight the potential feedback of the soil moisture in enhancing the intensities of the heat waves over this
229 region (Fisher et al. 2007, Mueller and Seviratne 2013, Miralles et al. 2014, Whan et al. 2015).

230 The main difference between the datasets is the higher occurrence of both heat and cold waves for ERAI than
231 the other datasets. This could be an effect of the coarser resolution in time and space of the reanalysis compared
232 to the ground observations that tends to smooth the temporal evolutions of the temperature anomalies and so
233 of the quantiles. Due to that lower temporal variability, the chance to get long term anomalies is increased
234 when using ERAI as compared to the other datasets.

235 As the total number of occurrences is the sum of all individual waves, the distribution of the wave durations
236 is needed to complete the picture. Fig. 6 displays the spatial variability of the last quartile of the wave durations
237 recorded for each grid point. It appears that the difference between the durations of heat and cold waves
238 between the three different datasets is much lower than the difference of occurrence discussed previously (Fig.
239 4 and 5). It is also interesting to note that, especially for cold waves, the regions where the waves are the most
240 frequent are not the same where they are the most persistent. Finally, it is remarkable to record many of the
241 longest durations of the cold waves along the coasts of the North Sea and the Baltic Sea. Indeed, the climate
242 along the coasts is generally more variable than in the continental regions, and so the waves are supposed to
243 be shorter. According to the same calculations using only Tmin and Tmax (not shown), the spatial



244 heterogeneity of the cold wave durations is much larger when T_{max} is used than T_{min} and we observe a strong
245 increase of the wave durations with T_{max} over northern Germany, Denmark, northern Poland, the Baltic Sea
246 and southern Scandinavia. That highlights the persistency of negative anomalies of T_{max} over these regions,
247 which could increase the chance to get longer durations with the intersection method and could explain the
248 results in Fig. 6.

249 3.2.2 Intensity of the heat and cold waves

250 The climatology of the intensities is important but very sensitive to the definitions applied in order to provide
251 a baseline and to calibrate the waves monitored, it is, therefore, important to analyse and justify the method
252 applied. The three methods, I1, I2 and I3 (using the quantiles, the temperature anomalies and the constant
253 threshold of temperature, see Sect. 2.2), are compared during heat and cold waves in Fig. 7. The distributions
254 of each scatter plot indicate the relationships by pairs in between the three methods for all the events, and the
255 colours indicate the corresponding durations of the events. Note that this figure is using LisFlood, but the same
256 results are obtained for the other datasets. These panels show the strong dependency of the intensities derived
257 from the quantiles and the durations (colour distribution well vertically distribute in Fig. 7b and horizontally
258 in Fig. 7c and 7e). This is especially true for the cold waves (correlations in between duration and I1 larger
259 than 0.95). These high correlations highlight the redundancy in the information with the wave durations.
260 Moreover, I1 is also climatologically bounded by the values recorded during the past period. For these reasons
261 the use of the quantiles appears not suitable to assess the heat and cold wave intensities. The methods derived
262 from the temperature anomaly (I2) and constant threshold (I3) are chosen. Indeed, the correlations in between
263 the wave durations and I2 and with I3 are much lower and not significant (on average 0.72 and 0.59), showing
264 the potential additional information provided. Moreover, these values are not bounded by the historical values
265 and so they will be able to better distinguish the most severe cases. According to the scatter plots in Fig. 7d
266 (for the heat waves) and Fig. 7f (for the cold waves), these methods appear quite independent at European
267 scale. Nevertheless the analyses of the correlations in between the methods a grip point level reveal a large
268 spatial variability (not shown). For instance, the correlations of I2 and I3 go up to 0.95 over France and
269 Western Russia, explained by heat (cold) waves occurred during the warmest (coldest) months, and go down
270 to 0.5 over Central and Northern Europe.

271 Except for the strongest events, there is an overall good agreement of the datasets to represent the probability
272 distribution functions (PDF) of the intensities of heat and cold waves. For instance, Fig. 8 display the
273 distribution of intensities defined by the method of the temperature anomalies (I2) and show no significant
274 difference for intensities lower than 60. This figure also confirms our finding of the higher occurrence of cold
275 waves than heat waves especially in the intensities larger than 25. In the tails of the distribution (especially
276 for the heat waves larger than 90), the differences are associated with a very low number of cases. The spatial
277 variability of these intensities I2 for the last 21 years was assessed by the strongest cold and heat waves
278 recorded over each grid point (Fig. 9). From this figure, the two strongest heat waves that occurred in Europe
279 can be clearly identified, namely the one that occurred in Russia in 2010 and the one in France in 2003. For
280 these two events, the intensities are slightly stronger using ERAI with both a longer duration and daily



281 intensities (not shown). For the cold waves, the intensities are stronger than the heat waves. The most intense
282 events occurred over the continental regions (Central Europe and South of Russia). The three datasets are well
283 in agreement for the intensities and the spatial variabilities. It is interesting to highlight that these intensities
284 are not well correlated to the occurrence, i.e., a region with more cases does not necessarily record the most
285 extreme events (Fig. 4 and 5). The relative short period of study (21 years) can generate some artefacts over
286 regions that recorded extraordinary events (especially true for Russia).

287 To assess the uncertainties relative to the methodology used, Fig. 10 display the same distributions but for
288 intensities calculated using constant thresholds (I3). Even if the scales are different, the spatial distribution of
289 I2 and I3 for the strongest heat waves are quite similar. The patterns are strongly influenced by the two heat
290 waves in 2003 and 2010. In opposite, the distribution of the strongest cold waves changes drastically. Whereas
291 the intensities over Russia are reduced, we note a relative increase of the intensities in Western Europe,
292 especially in North Germany, the Netherlands, and in Central Europe. As discussed previously, this
293 modification is explained by events that occurred more during the transitional months (intense I2 but not I3)
294 or close to the maximum (or minimum) seasonal temperature (intense I3). The spatial distribution is also
295 changed due to the normalisation according to the amplitude of the seasonal cycle, which is larger in
296 continental regions (not shown). Even if the results display significant differences according to the methods
297 and the regions, it is important to note that the three datasets are still well in agreement.

298 3.3 Return periods

299 As the purpose of this study is to provide a methodology that is useable for a monitoring system that must be
300 robust and understandable for users and decision makers, the information will be provided in terms of return
301 periods. This product will quantify, at monthly time scale, the intensity of the cold or heat waves that have
302 occurred. To build this indicator, all the days defined as cold or heat waves are summed for different
303 accumulation periods (from monthly to seasonally, see Table 3). Monthly values characterize either one
304 specific event as defined previously or several consecutives cases. As indicated by WMO (2015), intense or
305 repetitive extreme waves may have strong impacts on human health and so should be assessed. Once these
306 monthly values are calculated for each grid point, the return period can be estimated. Problem when dealing
307 with extremes are linked to erroneous extreme values and the sampling. To partially address these issues, we
308 have compared different datasets and different theoretical distributions have been fitted and tested on the
309 empirical distribution of the summed up intensities. This is done at grid point and at region level. In the
310 literature, different distributions have been tested such as the Gamma (Meehl et al. 2000) or the Weibull
311 distribution (Cueto et al 2010). According to the Pearson goodness-of-fit statistic, and the deviance statistic
312 on the entire distribution, the Gamma distribution is the most robust (not shown). By using the theoretical
313 distribution, the return periods can be extrapolated to durations longer than the duration of the initial time
314 series (21 years). Despite the non-stationarity of the climate, this relative short climate period reduces the
315 trend and allows the hypothesis of stationarity. Once the parameters of the Gamma distribution are estimated
316 for monthly, bimonthly and seasonal time scales (see table 3), return periods are calculated for both the cold



317 and heat waves. In that section, the results are produced using LisFlood dataset, which has been validated in
318 the previous section, but similar results are obtained with the two other datasets.

319

320 The boxplots (in Fig. 11) indicate the relationships between intensities and return periods over each grid point
321 in Europe. According to size of the inter quartiles, it appears the large spatial variabilities over the domain.
322 For instance, heat waves with intensities of 20 (10) using I2 (I3) have inter quartiles of return period that span
323 from 7 to 50 years (25 to 125 years respectively). Due to the more frequent intense cold waves, the return
324 periods are smaller than for the heat waves for similar intensities. The use of other datasets provide similar
325 results. Nevertheless, according to the previous findings, ERAI has less spatial variability (lower spread of the
326 boxes), and lower return periods due to the larger wave intensities recorded (not shown).

327

328 The spatial variabilities are then analysed in more detail with a region classification. This classification is a
329 simplification of the one reported in the EEA report (2016) that takes into account the climatology of the
330 regions (Continental, Mediterranean, Oceanic, Scandinavian, small panels in Fig. 11). Over these regions, the
331 calculation of return periods are assessed and compared (coloured dots in Fig. 11). Even if the results for the
332 two intensities (left and right panels) cannot be compared directly because the calculations are different, it is
333 interesting to compare the order of the regions according to the return periods. For heat waves, the British
334 Islands are remarkable by using the two intensities. The few intense heat waves recorded generate return
335 periods in the outliers of the box distribution in Europe. In opposite the Russian region records the lowest
336 return periods for similar intensities using I2 showing the large hazard of these heat waves in this region.
337 Nevertheless, the use of the I3 calculation (more sensitive to waves that occurred during the hearth of the
338 season) shows a different distribution with more cases over Central Europe for return periods lower than 5
339 years (in yellow) and the North-West European region (red) for the most intense heat waves. For the cold
340 waves, the British Islands and the Mediterranean regions are the least affected in the two intensity calculations,
341 whereas the continental parts of Europe (Russia and Central Europe) are associated with more regular intense
342 cold waves.

343 Based on these calculations, the monthly intensities are transformed into return periods, resulting in more
344 comprehensible information for users. In Fig. 12, the intensities of the heat and cold waves with a return period
345 of 10 years are plotted using I2 and I3. These values are sensitive to the distribution (number and intensities)
346 of the waves recorded during the 21 years analysed. That is why we observe the increase of intensity over
347 western Russia in Fig. 12 (left panels) where the waves are more frequent (Fig. 4 and 5) and more intense
348 (Fig. 9). The same results with I3 show a different behaviour Fig. 12 (right panels), mainly due to the change
349 of the most intense waves recorded and plotted Fig. 10. The potential impacts of these heat and cold waves
350 will be calculated regarding the absolute intensities and the return periods. But we could expect that identical
351 intensities of waves that occurred over two different regions and so with two different return periods may have
352 different impacts. For example, the absolute value of the heat wave intensity recorded in August 2003 over



353 France using I3 does not give extreme value regarding the intensities recorded in continental regions.
354 Nevertheless, the equivalent return value over France is larger than 50 years (not shown), in agreement with
355 Barriopedro et al. (2011) and Trigo et al. (2005), which suggest the potential strong risk associated.

356 Given the short period used in this study, the return periods cannot be as accurate as those ones reported in
357 previous studies, nevertheless, the information allows identifying the most extreme situations. The same
358 information is also available for the 2-month and seasonal time scales (not shown). The developed
359 methodology will allow to provide a robust and understandable indicator that is standardized by the local
360 climatology.

361

362 **4 Summary and Conclusions**

363 In this paper, we propose to monitor heat and cold waves by using a method based on the persistency of the
364 exceedance of quantiles of daily minimum and maximum temperatures at grid point level. In the first step, the
365 methods to detect and quantify the intensities of heat and cold waves were assessed. Tests were performed
366 with three methods: using the sum of the quantiles, the sum of the temperature anomalies regarding thresholds
367 depending the calendar days and the sum of the temperature anomalies regarding a constant threshold. The
368 sensibility tests on the influence of Tmin, Tmax and the intersection of both demonstrated the large influence
369 of using the two daily temperatures in decreasing drastically their frequencies. Finally three datasets were
370 compared, two derived from station data (LisFlood and EOBS) and one from reanalysis data (ERA-Interim). The two
371 observational datasets presented only minor differences in heat and cold waves occurrences and intensities.
372 This is probably due to the good agreement in between the two datasets for Tmin and Tmax. Using ERA-Interim
373 some differences appeared mainly due to the coarser resolution of the original grid and the use of only 4 values
374 per day to define Tmin and Tmax. In this case, the persistency and the spatial correlation were increased,
375 generating less spatial distinction and more intense waves than using the first two datasets. However, the main
376 results are in overall agreement for all three datasets and show an increased hazard for heat and cold waves in
377 the continental part of Europe. The data are also in agreement when transforming the intensities into return
378 periods. These relationships will be used operationally in the EDO website to provide robust and
379 comprehensible information for decision makers and users.

380 In perspective, these datasets and results should be compared to the results derived from forecast products in
381 view of providing a comprehensive and seamless tool for monitoring and forecasting heat and cold waves in
382 Europe.

383



384 **References**

385 Barriopedro, David, et al. "The hot summer of 2010: redrawing the temperature record map of Europe."
386 *Science* 332.6026 (2011): 220-224.

387

388 Budd, G. M. "The wet-bulb globe temperature: its history and limitations." *J. Science and Medicine in Sport*
389 11 (2009): 20-32.

390

391 Cueto, Rafael O. García, Adalberto Tejada Martínez, and Ernesto Jáuregui Ostos. "Heat waves and heat days
392 in an arid city in the northwest of Mexico: current trends and in climate change scenarios." *International*
393 *journal of biometeorology* 54.4 (2010): 335-345.

394

395 de'Donato FK, Leone M, Noce D, Davoli M, Michelozzi P (2013) The Impact of the February 2012 Cold Spell
396 on Health in Italy Using Surveillance Data. *PLoS ONE* 8(4): e61720. doi:10.1371/journal.pone.0061720

397

398 Dee, D. P., Uppala, S. M., Simmons, A. J., Berrisford, P., Poli, P., Kobayashi, S., and Bechtold, P. (2011).
399 The ERA-Interim reanalysis: Configuration and performance of the data assimilation system. *Quarterly*
400 *Journal of the royal meteorological society*, 137(656), 553-597.

401

402 De Roo, A. P. J., Wesseling, C. G., & Van Deursen, W. P. A. (2000). Physically based river basin modelling
403 within a GIS: the LISFLOOD model. *Hydrological Processes*, 14(11-12), 1981-1992.

404

405 Doblas-Reyes, F. J., M. J. Casado, and M. A. Pastor. "Sensitivity of the Northern Hemisphere blocking
406 frequency to the detection index." *Journal of Geophysical Research: Atmospheres* 107.D2 (2002).

407

408 EEA report (2016). *Climate Change, impacts and vulnerability in Europe in 2016, an indicator-based report.*
409 EEA report (1/2017). ISSN 1977-8449.

410

411 Fischer, E.M., S.I. Seneviratne, P.L. Vidale, D. Lüthi, & C. Schär (2007). Soil-Atmosphere interactions during
412 the 2003 European summer heat wave. *J. Clim.*, 5081-5099. DOI: 10.1175/JCLI4288.1

413

414 Gasparrini, Antonio, and Ben Armstrong. "The impact of heat waves on mortality." *Epidemiology*
415 (Cambridge, Mass.) 22.1 (2011): 68.

416

417 Haylock, M. R., Hofstra, N., Klein Tank, A. M. G., Klok, E. J., Jones, P. D., & New, M. (2008). A European
418 daily high-resolution gridded data set of surface temperature and precipitation for 1950–2006. *Journal of*
419 *Geophysical Research: Atmospheres*, 113(D20).

420



- 421 Hirschi, Martin, et al. "Observational evidence for soil-moisture impact on hot extremes in southeastern
422 Europe." *Nature Geoscience* 4.1 (2011): 17-21.
423
- 424 Kovats, R. Sari, and L. Ebi Kristie. "Heatwaves and public health in Europe." *The European Journal of Public
425 Health* 16.6 (2006): 592-599.
426
- 427 Kuglitsch, Franz G., et al. "Heat wave changes in the eastern Mediterranean since 1960." *Geophysical
428 Research Letters* 37.4 (2010).
429
- 430 Li, P. W., and S. T. Chan. "Application of a weather stress index for alerting the public to stressful weather in
431 Hong Kong." *Meteorological Applications* 7.04 (2000): 369-375.
432
- 433 Meehl, Gerald A., et al. "An introduction to trends in extreme weather and climate events: observations,
434 socioeconomic impacts, terrestrial ecological impacts, and model projections." *Bulletin of the American
435 Meteorological Society* 81.3 (2000): 413.
436
- 437 Miralles, D.G., A.J. Teuling, C.C. van Heerwarden & J. Vilà-Guerau de Arellano (2014). Mega-heatwave
438 temperatures due to combined soil desiccation and atmospheric heat accumulation. *Nature Geoscience*, vol.
439 7, May 2014, 345-348.
440
- 441 Mueller, B. and S. Seneviratne (2013). How soils send messages on heatwaves. *Global Change*, 81, October
442 2013.
443
- 444 Montero, J. C., et al. "Influence of local factors in the relationship between mortality and heat waves: Castile-
445 La Mancha (1975–2003)." *Science of the Total Environment* 414 (2012): 73-80.
446
- 447 Perkins, S. E., and L. V. Alexander. "On the measurement of heat waves." *Journal of Climate* 26.13 (2013):
448 4500-4517.
449
- 450 Porter, John R., and Mikhail A. Semenov. "Crop responses to climatic variation." *Philosophical Transactions
451 of the Royal Society B: Biological Sciences* 360.1463 (2005): 2021-2035.
452
- 453 Robine, Jean-Marie, et al. "Death toll exceeded 70,000 in Europe during the summer of 2003." *Comptes rendus
454 biologies* 331.2 (2008): 171-178.
455
- 456 Rocklov, Joacim, Adrian G. Barnett, and Alistair Woodward. "On the estimation of heat-intensity and heat-
457 duration effects in time series models of temperature-related mortality in Stockholm, Sweden." *Environmental
458 Health* 11.1 (2012): 1.



459

460 Rooney, Cleone, et al. "Excess mortality in England and Wales, and in Greater London, during the 1995
461 heatwave." *Journal of epidemiology and community health* 52.8 (1998): 482-486.

462

463 Russo, S., Dosio, A., Graversen, R. G., Sillmann, J., Carrao, H., Dunbar, M. B., and Vogt, J. V. (2014).
464 Magnitude of extreme heat waves in present climate and their projection in a warming world. *Journal of*
465 *Geophysical Research: Atmospheres*, 119(22).

466

467 Russo, Simone, Jana Sillmann, and Erich M. Fischer. "Top ten European heatwaves since 1950 and their
468 occurrence in the coming decades." *Environmental Research Letters* 10.12 (2015): 124003.

469

470 Schubert, Siegfried D., et al. "Northern Eurasian heat waves and droughts." *Journal of Climate* 27.9 (2014):
471 3169-3207.

472

473 Smoyer-Tomic, Karen E., Robyn Kuhn, and Alana Hudson. "Heat wave hazards: an overview of heat wave
474 impacts in Canada." *Natural hazards* 28.2-3 (2003): 465-486.

475

476 Sousa, P. M., Trigo, R. M., Barriopedro, D., Soares, P. M., & Santos, J. A. (2017). European temperature
477 responses to blocking and ridge regional patterns. *Climate Dynamics*, 1-21.

478

479 Steadman, Robert G. "The assessment of sultriness. Part I: A temperature-humidity index based on human
480 physiology and clothing science." *Journal of applied meteorology* 18.7 (1979): 861-873.

481

482 Steadman, Robert G. "A universal scale of apparent temperature." *Journal of Climate and Applied*
483 *Meteorology* 23.12 (1984): 1674-1687.

484

485 Tibaldi, S., et al. "Northern and Southern Hemisphere seasonal variability of blocking frequency and
486 predictability." *Monthly Weather Review* 122.9 (1994): 1971-2003.

487

488 Tomczyk, Arkadiusz M., and Ewa Bednorz. "Heat waves in Central Europe and their circulation conditions."
489 *International Journal of Climatology* 36.2 (2016): 770-782.

490

491 Trenberth, Kevin E., and John T. Fasullo. "Climate extremes and climate change: The Russian heat wave and
492 other climate extremes of 2010." *Journal of Geophysical Research: Atmospheres* 117.D17 (2012).

493

494 Trigo, R. M., García - Herrera, R., Díaz, J., Trigo, I. F., & Valente, M. A. (2005). How exceptional was the
495 early August 2003 heatwave in France?. *Geophysical research letters*, 32(10).



496

497 Van den Besselaar, E. J. M., Haylock, M. R., Van der Schrier, G., & Klein Tank, A. M. G. (2011). A European
498 daily high-resolution observational gridded data set of sea level pressure. *Journal of Geophysical Research:*
499 *Atmospheres*, 116(D11).

500

501 Van den Besselaar, E. J. M., Klein Tank, A. M. G., Van der Schrier, G., & Jones, P. D. (2012). Synoptic
502 messages to extend climate data records. *Journal of Geophysical Research: Atmospheres*, 117(D7).

503

504 Whan, K., J. Zscheischler, R. Orth, M. Shongwe, M. Rahimi, E.O. Asare, S.I. Seneviratne (2015). Impact of
505 soil moisture on extreme maximum temperatures in Europe. *Weather and Climate Extremes* 9 (2015) 57-67.

506

507 World Meteorological Organization, World Health Organization (2015) Heatwaves and health: guidance on
508 warning system development. WMO-No. 1142. [http://www.who.int/entity/globalchange/publications/Web-](http://www.who.int/entity/globalchange/publications/Web-release-WHO-WMO-guidance-heatwave-and-health.pdf?ua=1)
509 [release-WHO-WMO-guidance-heatwave-and-health.pdf?ua=1](http://www.who.int/entity/globalchange/publications/Web-release-WHO-WMO-guidance-heatwave-and-health.pdf?ua=1)

510

511 Zhang, X., Hegerl, G., Zwiers, F. W., & Kenyon, J. (2005). Avoiding inhomogeneity in percentile-based
512 indices of temperature extremes. *Journal of Climate*, 18(11), 1641-1651.



	HOT DAYS	DAYS IN HW	NUMBER OF HW
T_{MIN}	376 (17.9)	226 (31.8)	44.2 (5.1)
T_{MAX}	382 (10.7)	269 (31.0)	51 (4.9)
T_{INT}	150 (36.3)	81.3 (33.9)	16.9 (6.1)

513 Table 1 Spatial mean (and standard deviation in brackets) of number of days detected as hot days (larger than
 514 quantile 0.9, first column), over the entire period of analysis, days detected during heat waves (HW, with
 515 persistency longer than 3 days, second column) and total number of HW (third column) using only Tmin (first
 516 row), only Tmax (second row) and the intersection of the two variables (T_{int}, third row).

517

518

	COLD DAYS	DAYS IN CW	NUMBER OF CW
T_{MIN}	380 (20.8)	272 (30.5)	50 (5.3)
T_{MAX}	380 (14.8)	282 (27.4)	50.3 (4.3)
T_{INT}	196 (48.2)	128 (42.7)	25.2 (7.6)

519

520 Table 2 Same as Table 1 for the cold days and cold waves (CW).

521

522

Months	JAN	FEB	MAR	APR	MAY	JUN	JUL	AUG	SEP	OCT	NOV	DEC
Type	Cold	Cold	Cold	Heat	Heat	Heat	Heat	Heat	Heat	Cold	Cold	Cold
Duration	1, 2	1, 2	1, 2, S	1	1, 2	1, 2	1, 2	1, 2	1, 2, S	1	1, 2	1, 2

523

524 Table 3 Type of wave calculated operationally at the end of every Month. The period in which the intensities
 525 are calculated are indicated in the last row (1 for 1 month, 2 for 2 months or S for Season, i.e. 6 months).

526



527 **List of figures**

528 Figure 1 Schema of the detection method and the calculation of the intensities of heat waves, based on temperature anomalies of a
529 calendar day threshold: Q90(Tmax) and Q90(Tmin) (I2 calculation), or based on the constant climatological threshold defined by
530 the median of the daily quantiles: Med(Q90(Tmax)) and Med(Q90(Tmin)) (I3 calculation). 18

531 Figure 2 Temporal correlation of the temperature quantiles of Tmin (first row), and Tmax (second row) provided by ERAI, EOBS
532 and LisFlood datasets from 1995 to 2015. The datasets compared are indicated on the top of each column. 19

533 Figure 3 Mean Absolute Error of temperature (in K) between the three datasets, calculated from 1995 to 2015 for Tmin (first row)
534 and Tmax (second row). The datasets compared are indicated on the top of each column. 20

535 Figure 4 Number of occurrences of heat waves in Europe from 1995 to 2015 using the intersection of both Tmin and Tmax (Tint,
536 first row), only Tmin (second row), and only Tmax (third row) with LisFlood (first column), E-OBS (second column) and ERAI
537 (third column) datasets. 21

538 Figure 5 Number of occurrences of cold waves in Europe from 1995 to 2015 using the intersection of both Tmin and Tmax (Tint,
539 first row), only Tmin (second row), and only Tmax (third row) with LisFlood (first column), E-OBS (second column) and ERAI
540 (third column) datasets. 22

541 Figure 6 Last quartile of the wave durations (in days) for the heat (top panels) and cold (bottom panels) waves using LisFlood, E-
542 OBS and ERAI datasets. 23

543 Figure 7 Matrix of scatter plots of the three intensity calculations related to quantiles, temperature anomalies and temperatures
544 anomalies with constant thresholds (I1, I2 and I3 respectively) during heat (a, b, d) and cold (c, e, f) waves using LisFlood. The
545 colours indicate the duration (in days) of each wave. 24

546 Figure 8 Histograms of heat (left panel) and cold (right panel) waves intensities defined as temperature anomalies (I2) for the three
547 datasets. Note that the frequency axis are on a Log-scales. 25

548 Figure 9 Spatial distribution of the strongest heat (top panels) and cold (bottom panels) waves intensities, defined as temperature
549 anomalies (I2), using LisFlood, E-OBS and ERAI datasets. 26

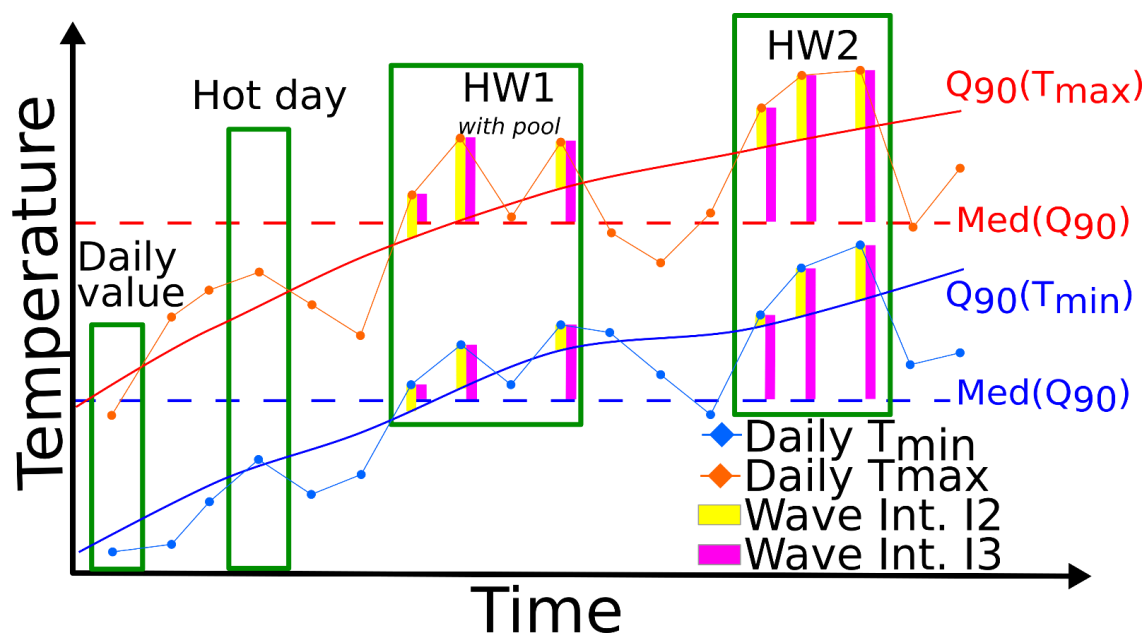
550 Figure 10 Same as Fig. 9 using the intensity based on the constant threshold (I3) for heat (top panels) and cold (bottom panels)
551 waves, and based on LisFlood (first row), E-OBS (second row) and ERAI (third row). 27

552 Figure 11 Return periods of monthly intensities of heat (top) and cold (bottom panels) waves for two intensities (I2, left panels and
553 I3, right panels). Boxes assess the spatial variability for the grid points. Coloured dots indicate the return period calculated over the
554 regions defined in the small panels. 28

555 Figure 12 Intensity of the heat (top panels) and cold (bottom panels) waves defined with the temperature anomalies (I2, left panels),
556 or with constant thresholds (I3, right panels) with a 10-year return period using LisFlood dataset. 29

557

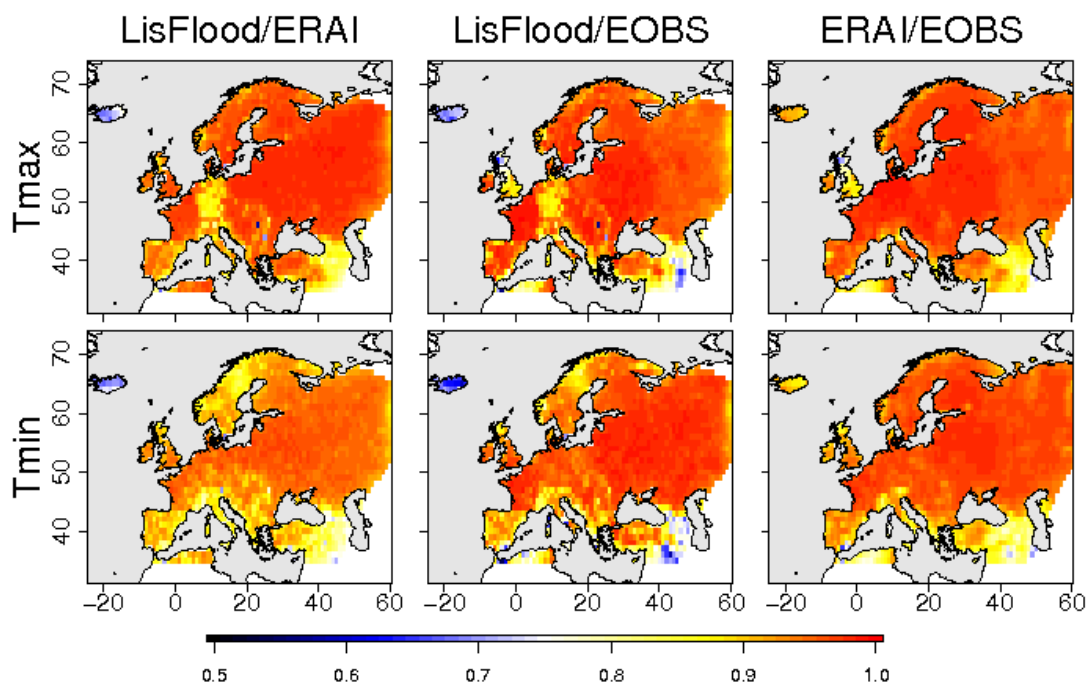
558



559

560 Figure 1 Schema of the detection method and the calculation of the intensities of heat waves, based on
 561 temperature anomalies of a calendar day threshold: Q_{90} of both T_{max} and T_{min} (I2 calculation), or based
 562 on the constant climatological threshold defined by the median of the daily quantiles: $Med(Q_{90})$ of both
 563 T_{max} and T_{min} (I3 calculation).

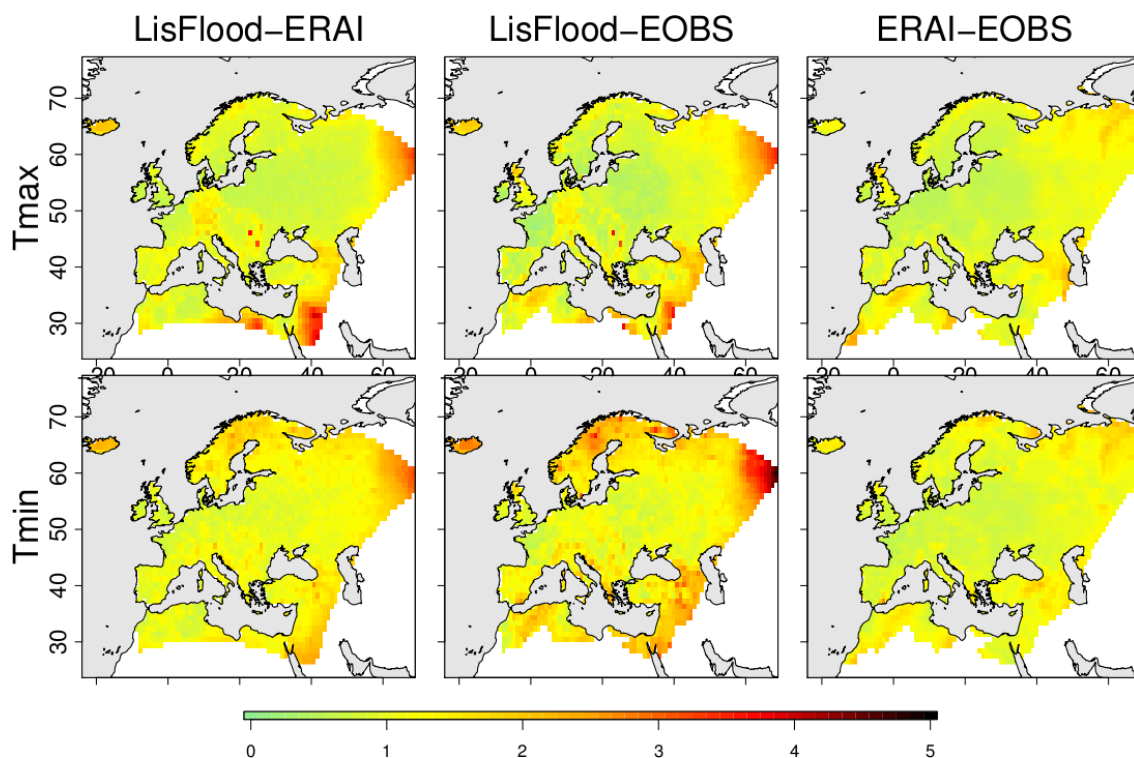
564



565

566 Figure 2 Temporal correlation of the temperature quantiles of Tmin (first row), and Tmax (second row)
567 provided by ERA1, EOBS and LisFlood datasets from 1995 to 2015. The datasets compared are indicated on
568 the top of each column.

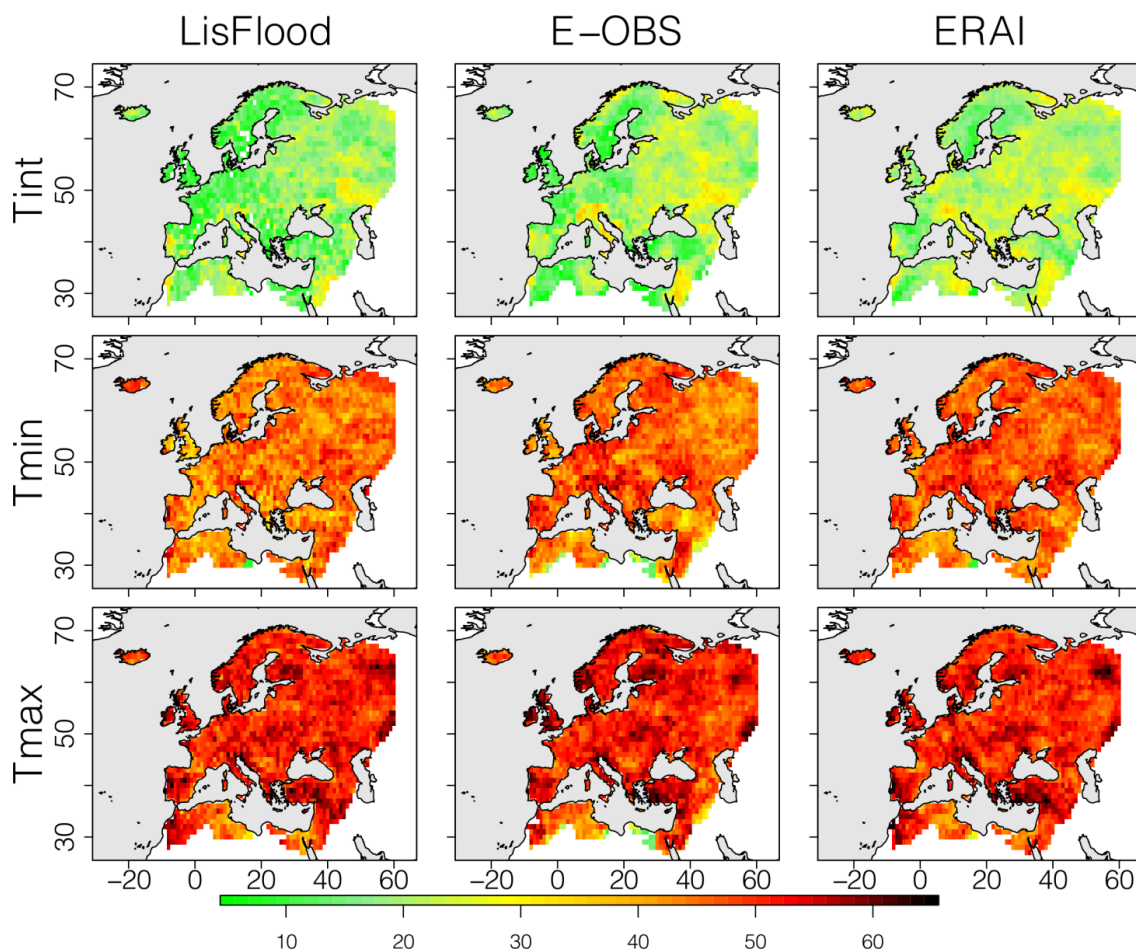
569



570

571 Figure 3 Mean Absolute Error of temperature (in K) between the three datasets, calculated from 1995 to
572 2015 for Tmin (first row) and Tmax (second row). The datasets compared are indicated on the top of each
573 column.

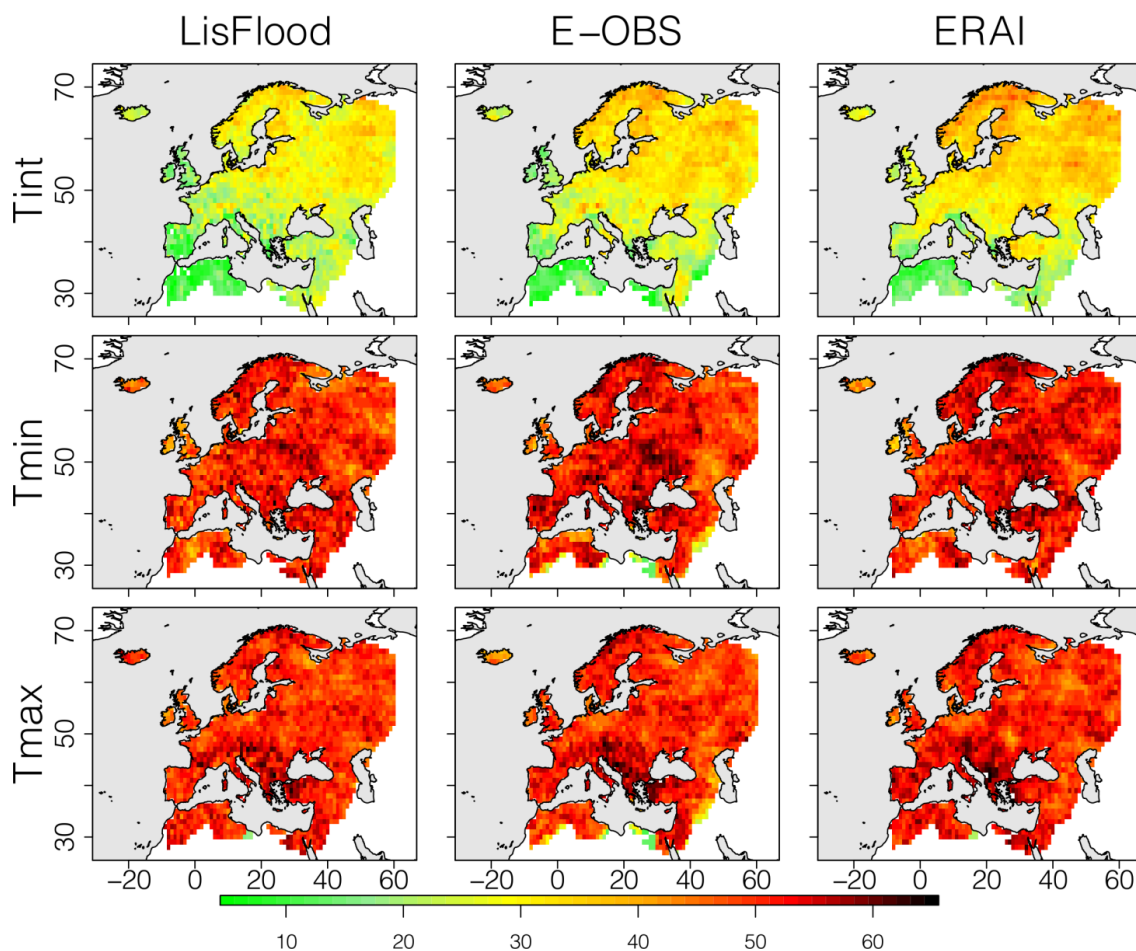
574



575

576 Figure 4 Number of occurrences of heat waves in Europe from 1995 to 2015 using the intersection of both
577 Tmin and Tmax (Tint, first row), only Tmin (second row), and only Tmax (third row) with LisFlood (first
578 column), E-OBS (second column) and ERAI (third column) datasets.

579



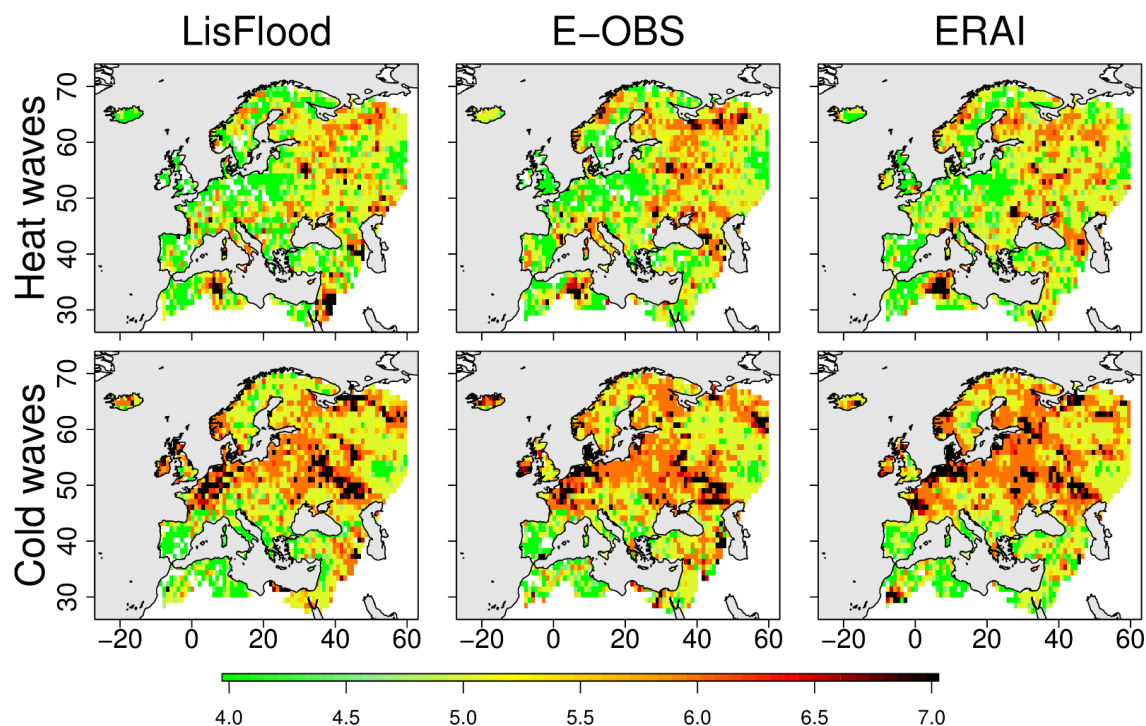
580

581 Figure 5 Number of occurrences of cold waves in Europe from 1995 to 2015 using the intersection of both
582 Tmin and Tmax (Tint, first row), only Tmin (second row), and only Tmax (third row) with LisFlood (first
583 column), E-OBS (second column) and ERAI (third column) datasets.

584



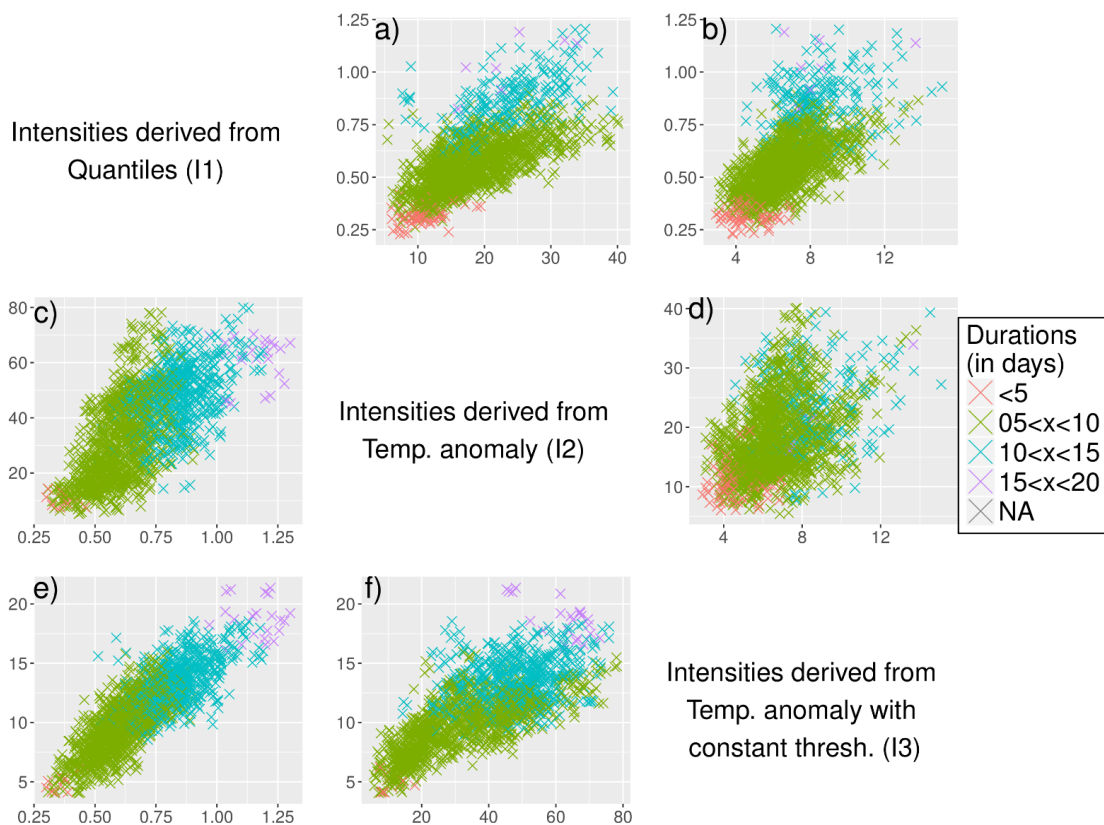
585



586

587 Figure 6 Last quartile of the wave durations (in days) for the heat (top panels) and cold (bottom panels) waves
588 using LisFlood, E-OBS and ERAI datasets.

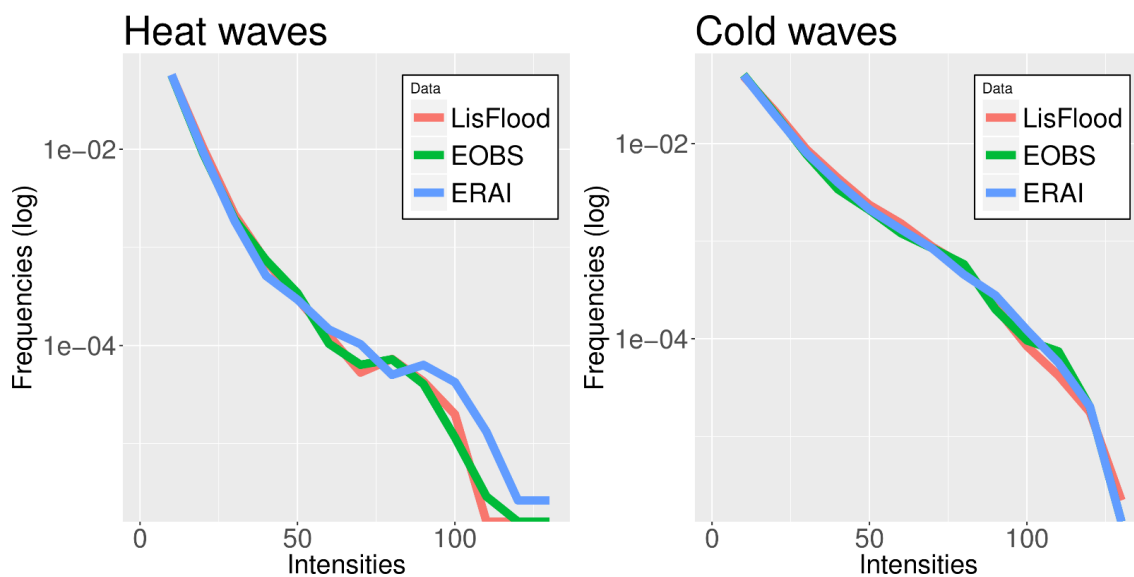
589



590

591 Figure 7 Matrix of scatter plots of the three intensity calculations related to quantiles, temperature anomalies
592 and temperatures anomalies with constant thresholds (I1, I2 and I3 respectively) during heat (a, b, d) and cold
593 (c, e, f) waves using LisFlood. The colours indicate the duration (in days) of each wave.

594



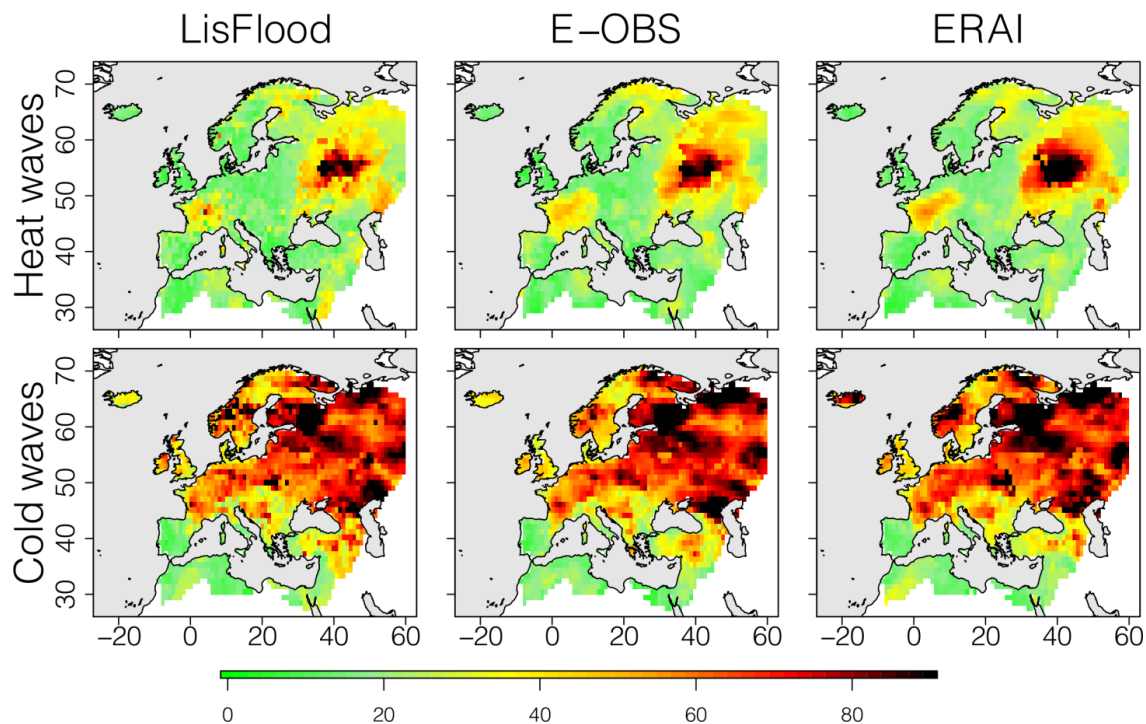
595

596 Figure 8 Histograms of heat (left panel) and cold (right panel) waves intensities defined as temperature
597 anomalies (I_2) for the three datasets. Note that the frequency axis are on a Log-scales.

598



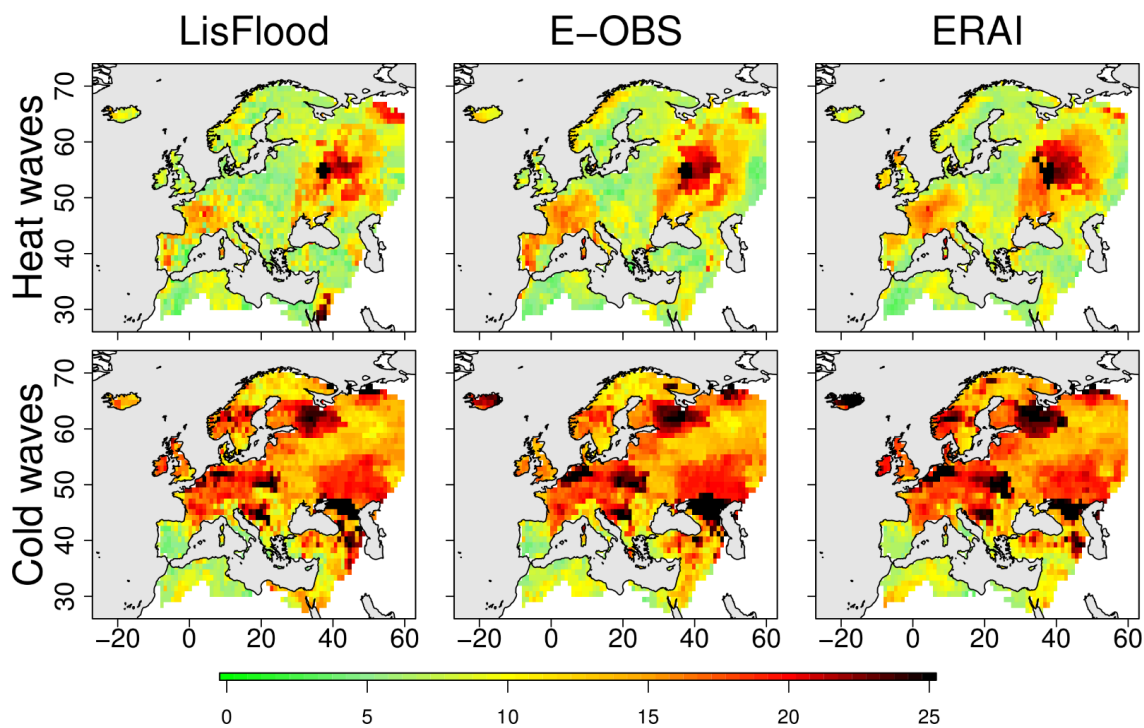
599



600

601 Figure 9 Spatial distribution of the strongest heat (top panels) and cold (bottom panels) waves intensities,
602 defined as temperature anomalies (I2), using LisFlood, E-OBS and ERAI datasets.

603



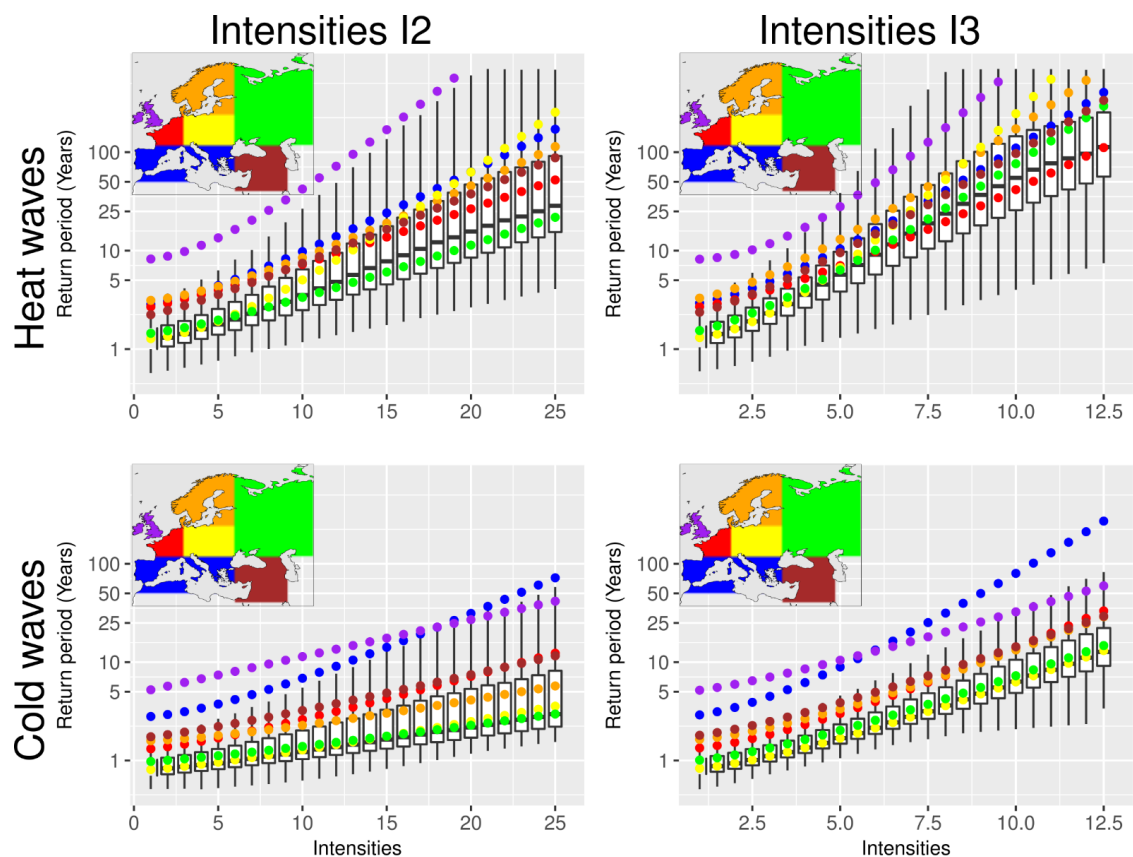
604

605

606

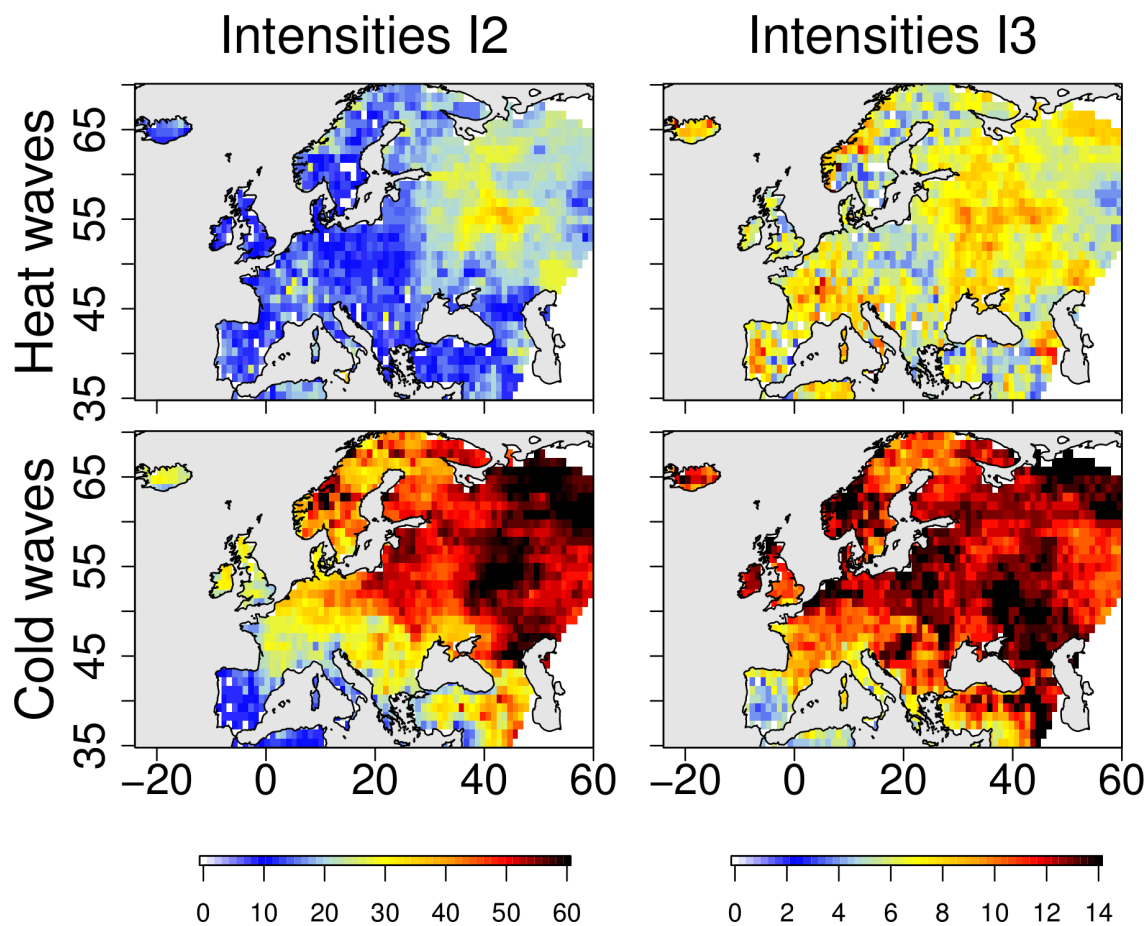
607

Figure 10 Same as Fig. 9 using the intensity based on the constant threshold (I_3) for heat (top panels) and cold (bottom panels) waves, and based on LisFlood (first row), E-OBS (second row) and ERAI (third row).



608

609 Figure 11 Return periods of monthly intensities of heat (top) and cold (bottom panels) waves for two intensities
610 (I2, left panels and I3, right panels). Boxes assess the spatial variability for the grid points. Coloured dots
611 indicate the return period calculated over the regions defined in the small panels.



612

613 Figure 12 Intensity of the heat (top panels) and cold (bottom panels) waves defined with the temperature
614 anomalies (I2, left panels), or with constant thresholds (I3, right panels) with a 10-year return period using
615 LisFlood dataset.